Original Paper

A dynamic managed pressure well-control method for rapid treatment of gas kick in deepwater managed pressure drilling

Hong-Wei Yang [a], Jun Li [a, b, *], Ji-Wei Jiang [c], Hui Zhang [a], Bo-Yun Guo [d], Geng Zhang [a], Wang Chen [a]

[a] China University of Petroleum-Beijing, Beijing, 102249, China
[b] China University of Petroleum-Beijing at Karamay, Karamay, 834000, Xinjiang, China
[c] CNPC Engineering Technology R & D Company Limited, Beijing, 102206, China
[d] University of Louisiana at Lafayette, Lafayette, LA, 70504, USA

ARTICLE INFO

ABSTRACT

During deepwater managed pressure drilling (MPD), the gas kick may occur in abnormally high-pressure formations. If the traditional well control method is adopted, the treatment time is long and the advantage of early gas kick detection of MPD is lost. The dynamic managed pressure well-control (MPWC) method can be used to rapidly treat gas kick in deepwater MPD. In this paper, considering the effect of large-variable-diameter annulus and complex wellbore temperature in deepwater drilling, a simplified model of non-isothermal gas—liquid two-phase flow was established for dynamic deepwater MPWC simulation. Using this model, the response characteristics of outlet flow and wellhead back-pressure were investigated. The results indicated that the gas fraction, outlet liquid flow rate, pit gain and wellhead backpressure presented complex alternating characteristics when gas moved upwards in the wellbore due to the large-variable-diameter annulus. The outlet liquid flow rate would be lower than the inlet flow rate and the pit gain would decrease before the gas moved to the wellhead. The variation trend of the wellhead backpressure was consistent with that of the pit gain. When the gas—liquid mixture passed through the choke, the expansion or compression of the gas caused part of the choke pressure drop to be supplemented or unloaded, delaying the response rate of the wellhead backpressure. The wellbore temperature, borehole diameter and seawater depth had different effects on outlet flow rate, pit gain and wellhead backpressure. This research could provide a new idea for well control methods in deepwater managed pressure drilling.

© 2022 The Authors. Publishing services by Elsevier B.V. on behalf of KeAi Communications Co. Ltd. This is an open access article under the CC BY-NC-ND license (http://creativecommons.org/licenses/by-nc-nd/4.0/).

1. Introduction

About 40% of global marine oil-gas resources are distributed in deepwater areas, and nearly 90% of the ocean is deeper than 1000 m (Randolph et al., 2011). Therefore, deepwater oil-gas resources are rich and have become a hot spot for exploration and development of marine oil-gas. However, the deepwater formation is different from the land formation or offshore formation. The seawater depth varies greatly and the temperature environment is special. Many challenges are faced during drilling, which are mainly manifested as complex formation pressure distribution, narrowly safe density window, difficult wellbore pressure control, frequent gas kick accidents, and small kick tolerance, etc. (Jiang et al., 2019; Nayeem et al., 2016). Managed pressure drilling (MPD) technology effectively solves the difficult drilling problem in deepwater formation, and it has been gradually promoted in deepwater drilling in recent years (Kaasa et al., 2012; Sule et al., 2018). However, when drilling into an abnormally high-pressure formation, the gas kick accident may still occur during MPD. It may cause the fluid invading into the wellbore to blow out of the wellhead if not handled in time, posing a great threat to drilling safety.

Well control is a key means to deal with gas kick (Ma et al., 2018; Vajargah and van Oort, 2015). When gas kick occurs, reasonable design of well control parameters and precise control of the well killing system can safely circulate the gas out of the wellbore and

* Corresponding author. China University of Petroleum-Beijing, Beijing, 102249, China.
E-mail address: lijun446@vip.163.com (J. Li).

Nomenclature

A	Annulus area, m^2
A_0	Heat transfer resistance of the annulus fluid to the surrounding environment
A_e	Distribution coefficient under bubble flow and slug flow
B_0	Heat transfer resistance of the annulus fluid to the drill string
c	Propagation rate of the pressure wave, Pa/s
c_0	Distribution coefficient
C_p	Specific heat capacity, J/(kg K)
C_t	Total compression factor, 1/MPa
C_v	Choke coefficient, m^2
d_c	Equivalent diameter of the annulus, m
E_g	Local gas expansion term
f	Friction coefficient
g	Gravity acceleration, m^2/s
h	Opening thickness of the reservoir, m
h_c	Convective heat transfer coefficient at the inner walls of the casing, W/(m^2 °C)
h_{pi}	Convective heat transfer coefficient at the inner walls of the drill string, W/(m^2 °C)
h_{po}	Convective heat transfer coefficient at the outer walls of the drill string, W/(m^2 °C)
h_{sea}	Convective heat transfer coefficient at the outer walls of the riser, W/(m^2 °C)
H	Well depth, m
H_w	Seawater depth, m
K	Reservoir permeability, D
m	Mass flow rate of the gas kick, kg/(m s)
m_c	Mass flow rate of the two-phase mixture, kg/s
m_g	Gas kick rate, kg/(m s)
m_g*	Gas kick rate term
P	Wellbore pressure, Pa
P_b	Bottomhole pressures, MPa
P_c	Wellhead backpressure, Pa
P_e	Reservoir pressures, MPa
P_s	Outlet pressure of the choke, Pa
q_c	Outlet liquid flow rate, m^3/s
q_g	Gas kick rate, m^3/s
q_L	Pump rate, m^3/s
r	Radius, m
r_{ci}	Inside radius of the casing, m
r_{co}	Onside radius of the casing, m
r_{pi}	Inside radius of the drill pipe, m
r_{po}	Onside radius of the drill pipe, m
r_{ri}	Inside radius of the riser, m
r_{ro}	Onside radius of the riser, m
r_w	Wellbore radius, m
R_g	Gas constant, J/(mol K)
S	Source term
t	Time, s
T	Wellbore temperature, °C
T_e	Surrounding environment temperature, °C
T_{EG}	The term accounting for the gas expansion in the well
T_D	Dimensionless temperature equation of the formation
T_p	Temperature inside the drill string, °C
T_{XE}	The expansion volume per unit time during gas moving from the bottomhole to the wellhead, m^3/s
U_a	Integrated convective heat transfer coefficient between the annulus and sea water, W/(m^2 °C)
U_p	Integrated convective heat transfer coefficient between the annulus and drill string, W/(m^2 °C)
v	Flow rate, m/s
v_c	Gas characteristic rate, m/s
v_∞	Slip rate, m/s
V	Annulus volume, m^3
Y	Gas expansion factor
z	Axial space, m
z_e	Gas compression factor under reservoir conditions
z_g	Gas compressibility factor
z_{op}	Choke opening

Greek letters

α	Volume fraction
χ	Decreasing term of the profile coefficient
γ	Adiabatic gas constant
λ_c	Thermal conductivity of the casing and riser, W/(m °C)
λ_{ce}	Thermal conductivity of the cement ring, W/(m °C)
λ_f	Thermal conductivity of the formation, W/(m °C)
λ_p	Thermal conductivity of the drill string, W/(m °C)
λ_r	Thermal conductivity of the seawater, W/(m °C)
μ	Viscosity, Pa s
θ	Well inclination angle, rad
ξ	Variable of integration, meaningless
ρ	Density, kg/cm^3

Subscript

g	Gas
L	Drilling fluid
m	Gas−liquid mixed fluid

return the drilling to normal. Traditional well control methods mainly include driller's method, engineer method and some other special well-killing methods. Many scholars have conducted a lot of theoretical research in the early stage. Leblanc and Lewis (1968) developed the first multiphase flow model for gas influx simulation, but the model neglected the effects of fluid friction and interphase slip between gas and liquid. Nickens (1987) applied the numerical solution scheme to solve the partial differential equations for the two-phase flow. He conducted a simulation of dynamic gas kick treatment after the formation gas entered the wellbore, and compared the advantages and disadvantages of the driller's method and the engineer method. Santos (1991) improved the Nickens's well control model to make it suitable for the well control calculation in horizontal wells. Rommetveit and Vefring (1991)

presented a multi-component gas kick model containing liquid, free gas, oil, and dissolved gas, and the simulation results were verified using actual measured data from full-scale test wells. Choe (2001) developed a dynamic well control model based on a combination of gas−liquid slippage, drilling fluid compressibility and annulus pressure loss. Using this model, the effects of various factors on pit gain and wellhead casing pressure were investigated. Nunes et al. (2002) developed a well kick analytical model, and calculated the annulus pressure distribution and gas fraction at each time step. Avelar et al. (2009) carried out a well control simulation of the deepwater driller's method using the drift flow model, and the results showed that the calculated outlet flow rate, pit gain, and annulus pressure agreed well with the experimental measurements. Manikonda et al. (2019) developed a semi-

analytical model to simulate the gas kick behavior utilizing various concepts, including gas solubility in oil-based drilling fluids. Also, they presented a simple mechanistic model and to describe a gas kick in a drilling riser with water-based mud and synthetic-based mud (Manikonda et al., 2020) and established a rigorous, mechanistic model for gas kick simulation, that used the thermodynamic approach to account for gas solubility in synthetic-based mud (Manikonda et al., 2021).

In MPD, the downhole measurement while drilling can dynamically monitor the bottomhole pressure or the wellhead micro-flow instrument can dynamically measure the variation in the outlet rate. Therefore, the gas kick can be identified when a small amount of gas influx comes into the bottomhole, significantly reducing the difficulty of well control (Jiang et al., 2019; Sule et al., 2019; Wang et al., 2020). However, if the traditional well control methods are adopted, the well needs to be shut in first, and the gas circulating and discharging is started when the standpipe pressure and casing pressure are no longer increasing. During this process, the gas will continue to enter the wellbore, although the gas kick rate gradually decreases to zero. Therefore, traditional well control methods not only take a long time for gas kick treatment, but also may cause small-scale gas kick to evolve into medium or large-scale gas kick, losing the advantage of early gas kick detection in MPD and increasing the difficulty of well control. With the development of MPD technology, a novel approach for rapid gas influx treatment on the basis of the dynamic control strategy of wellhead backpressure, i.e., dynamic managed pressure well-control (MPWC) method, has been gradually formed in recent years. It can control the wellhead choke manifold system to achieve a new balance of bottomhole-formation pressure without shutting in when gas kick is detected, and completely circulate the formation fluid entering the wellbore out of the wellhead (Das et al., 2008; Davoudi et al., 2011; Guner, 2009; Jiang et al., 2019; Kinik et al., 2014; Liao et al., 2020; Smith and Patel, 2012). The current investigation could be divided into two stages:

The first stage was the applicability exploration of the dynamic MPWC method. Das et al. (2008) analyzed the response characteristics of key parameters during dynamic MPWC based on the multiphase flow model. It was found that, compared to traditional well control methods, establishing a new pressure balance at the bottomhole by rapidly increasing the wellhead backpressure could reduce the wellbore pressure at the casing shoe, thereby reducing the mud loss risk in the formation with a narrowly safe density window. Guner (2009) compared the operating procedures, gas discharge volume and well control treatment time between the dynamic MPWC method and the traditional well control method. The results revealed that when the dynamic MPWC method was used to deal with gas kick, less formation gas entered the wellbore, and it was less difficult to circulate the gas out of the wellbore. Davoudi et al. (2011) compared the gas kick treatment effects by increasing the wellhead backpressure and increasing the pump rate based on the dynamic MPWC method. The results demonstrated that the method of increasing the wellhead backpressure could quickly and effectively establish the bottomhole-formation pressure balance, and safely circulate the gas out of the wellhead. Although the method of increasing the pump rate could increase the bottomhole pressure, the ability to deal with gas kick was very limited, which could easily lead to secondary gas kick accident and increase the difficulty of well control. Considering the well kick tolerance, rated pressure of well control equipment, well configuration, and amount of gas kick, Smith and Patel (2012) proposed a procedure for gas kick treatment using dynamic MPWC method, including early gas kick detection, well shut-in, well control method switching, etc. Jiang et al. (2019) explored how to apply the dynamic MPWC method to deepwater drilling to expand the limitation of well control.

The second stage was the simulation of the responses of key parameters during MPWC. Kinik et al. (2014) investigated the responses of standpipe pressure, wellhead backpressure, choke opening, outlet flow rate, and pit gain during dynamic MPWC, and compared with the traditional well control method to highlight the advantage of the dynamic MPWC method for gas kick treatment. Liao et al. (2020) established a gas−liquid-solid three-phase flow model to study the response characteristics of wellhead backpressure and outlet flow rate during dynamic MPWC.

The above analysis indicated that it was not only shorter but also less difficult to deal with gas kick using the dynamic MPWC method in MPD. However, as a new method, the current research was not sufficient, mainly in two aspects: (i) the current research mainly focused on the land drilling, where the wellbore conditions were simpler than those of deepwater drilling; (ii) few studies conducted on the response characteristics of outlet flow and wellhead backpressure, especially for deepwater drilling which have not been reported in the literature.

To this end, based on the dynamic MPWC method for rapid treatment of gas kick in deepwater MPD, a simplified model of nonisothermal gas−liquid two-phase flow was developed for dynamic MPWC simulation considering the large-variable-diameter annulus and the complicated wellbore temperature. Then, the response characteristics of outlet flow and wellhead backpressure were investigated, along with the sensitivity to the wellbore temperature, large-variable-diameter annulus, borehole diameter in formation section, and seawater depth. This study could provide a safe, fast and feasible implementation idea for gas kick treatment in deepwater MPD.

2. Dynamic deepwater MPWC method

During drilling in the deepwater formation with a narrowly safe density window using MPD technique, gas kick can be detected early if formation gas influx comes into the wellbore. Currently, the amount of gas in the wellbore is usually small, and the well control is less difficult. Therefore, this paper proposes a dynamic MPWC method for rapid treatment of gas kick in deepwater MPD, i.e., the choke manifold system of MPD is used to provide a certain wellhead backpressure and the gas in the wellbore is dynamically circulated out of the wellhead to return the drilling to normal. The dynamic MPWC method consists of four main stages: (i) gas influx into the wellbore during gas kick, (ii) rapid increase in wellhead backpressure to establish a new balance of bottomhole-formation pressure, (iii) dynamic control of wellhead backpressure to circulate the gas out of the wellbore, and (iv) resumption of normal drilling or circulation of weighted drilling fluid, as shown in Fig. 1. The details are as follows.

- The gas kick stage is shown in Fig. 1(a). During MPD in deepwater, the gas from abnormally high-pressure formation comes into the wellbore. The gas kick can be identified by decreasing bottomhole pressure or increasing outlet flow rate.
- The stage of establishing a new equilibrium between bottomhole pressure and formation pressure is shown in Fig. 1(b). Quickly adjust the choke opening and increase the wellhead backpressure to make the inlet and outlet flow rate the same, which means that the bottomhole-formation pressure has regained equilibrium and the gas has stopped entering the bottomhole.
- The stage of circulating the gas out of the wellbore is shown in Fig. 1(c)−(e). After the gas kick stops, it is necessary to circulate the drilling fluid to completely discharge the gas in the wellbore,
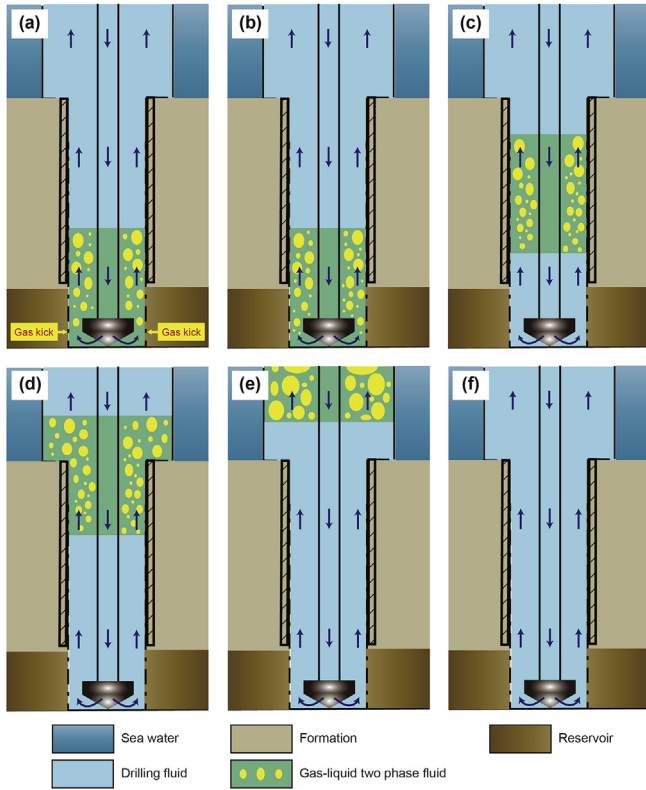
Fig. 1. Different stages during gas kick treatment using the dynamic deepwater MPWC method.

during which the wellhead backpressure must be dynamically adjusted to ensure a constant bottomhole pressure.

- The stage of resuming normal drilling or circulating the weighted drilling fluid is shown in Fig. 1(f). When the gas is completely discharged from the wellbore, if the wellhead backpressure is high, it is necessary to circulate the heavy drilling fluid to reduce the wellhead backpressure. Conversely, drilling can continue.

Deepwater MPD is different from land MPD. It not only has a special temperature environment, but also the large-sized riser will cause a large-variable-diameter flow channel in the annulus. These two factors have an important impact on the variations in the outlet flow and wellhead backpressure during gas kick treatment using the dynamic deepwater MPWC method.

3. Model development

The multiphase flow models usually include the drift flow model, two-fluid model, and homogeneous flow model (Flores et al., 1998; Petalas and Aziz, 2000; Ramos, 1995). The drift flow model takes into account the gas–liquid interphase slippage and the distribution of gas fraction and flow rate across the flow path, which makes the two-phase flow calculation error reduced and the solution relatively simple (Hasan and Kabir, 1988; Yang et al., 2019a, 2020). It has been widely used in gas kick and well control simulation (He et al., 2015; Yang et al., 2019b; Yin et al., 2017). However, the solution speed of the fully transient drift flow model is still slow, and it is not suitable for the real-time decision-making of key parameters during dynamic MPWC.

The pressure wave propagation rate in multiphase flow is much greater than that of the volume wave, and the effects of gas

migration on the wellbore pressure and flow characteristics are of even greater concern during well control. Therefore, based on this idea, many previous studies imposed a quasi-equilibrium momentum conservation equation instead of the transient momentum conservation equation, simplifying the fully transient drift flow model (Baer and Nunziato, 1986; Choi et al., 2013; Flatten and Lund, 2011). This simplified idea improved the calculation speed of the model under the condition of ensuring the required calculation accuracy. Therefore, in this paper, we propose to introduce the Aarsnes' (Aarsnes et al., 2016a, 2016b) simplified idea to develop a simplified model of non-isothermal gas–liquid two-phase flow. The main assumptions include:

(1) The fluids flow along the axial direction in the wellbore, regardless of its radial behavior;
(2) Treat the drilling fluid and cuttings as the liquid phase without considering the effect of cuttings separately;
(3) In the vertical wellbore, the pressures of the gas and the liquid on the same cross-section are considered to be the same, along with the temperature;
(4) The gas solubility in water-based mud is very small, and the mass transfer between gas and liquid is not considered;
(5) The heats generated from bit, torque, and frictions loss are neglected.

3.1. Hydrodynamic model

Aarsnes et al. ignored the flow channel diameter when simplifying the drift flow model. Thus, the model cannot adapt to the large-variable-diameter annulus in deepwater drilling (Aarsnes et al., 2016a, 2016b). To this end, the simplification of the drift flow model in this paper considers the effect of the annulus area, and the detailed derivation process can be found in Appendix A. The main governing equations are as follows.

The partial differential equation of the gas volume fraction considering the variation in annulus area is:

$$\frac{\partial (A\alpha_g)}{\partial t} + v_g \frac{\partial (A\alpha_g)}{\partial z} = E_g + m_g^* \tag{1}$$

with

$$E_g = -\frac{A\alpha_g (1 - c_0 \alpha_g)}{\gamma P}\left[\frac{\partial P}{\partial t} + v_g \frac{\partial P}{\partial z}\right] \tag{2}$$

$$m_g^* = \frac{(1 - c_0 \alpha_g)c_g^2}{\gamma P} m_g \tag{3}$$

Neglecting the transient acceleration, the wellbore pressure, consisting of the hydrostatic pressure, annulus pressure loss and wellhead backpressure, is:

$$P(z) = P_c + \int_H^z \overline{S}(\xi)\mathrm{d}\xi \tag{4}$$

$$\overline{S} = -\overline{\rho}_m\left(g \sin \theta + \frac{2f v_m |v_m|}{d_c}\right) \tag{5}$$

$$\overline{\rho}_m = \alpha_L \rho_L + \alpha_g \overline{\rho}_g \tag{6}$$

Regarding the entire annulus as a control volume unit, the wellhead backpressure can be expressed as an ordinary differential equation according to the law of mass conservation, i.e.

$$\frac{\partial P_c}{\partial t} = \frac{\overline{\beta}}{V}\left(q_L + q_g - q_c + T_{XE}\right) \tag{7}$$

with

$$\overline{\beta} = \frac{\beta_L}{1 + \frac{\beta_L}{V}\int_0^H \frac{c_0 \alpha_g(\xi)}{\gamma P(\xi)}\mathrm{d}\xi} \tag{8}$$

$$T_{XE} = A\left(v_g(H) - v_{g0}\right) \tag{9}$$

The gas migration rate in the annulus can be expressed as:

$$v_g(z) = e^{-I_v(z)}\left[v_{g0} + c_0\int_0^z\left(\frac{c_g^2(\xi)m_g(\xi)}{A\gamma P(\xi)}e^{I_v(\xi)}\right)\mathrm{d}\xi\right] \tag{10}$$

with

$$I_v(z) = \int_0^z\left[\frac{c_0\alpha_g(\xi)}{\gamma P(\xi)}\overline{S}(\xi)\right]\mathrm{d}\xi \tag{11}$$

$$v_{g0} = c_0\left(\frac{m_g}{A\rho_g} + v_L\right) + v_\infty \tag{12}$$

The above Eqs. ((1), (4), (7) and (10)) constitute the main governing equations of the simplified drift flow hydraulic model, which can be used to simulate the gas–liquid two-phase flow during dynamic MPWC. For other boundary conditions, please refer to Appendix A.

3.2. Thermodynamic model

Previous studies based on Aarsnes' simplified drift flow model did not consider the effect of temperature. As shown in Fig. 2, deepwater drilling has a special temperature environment, where the temperature gradient in the seawater section is opposite to the geothermal gradient. The temperature and pressure have a large effect on the gas–liquid physical parameters. In turn, variation of

Fig. 2. Schematic of heat transfer and ambient temperature in deepwater drilling.

physical fluid parameters can also affect the multiphase flow state and the wellbore pressure. Therefore, the coupling effect of wellbore temperature-pressure and fluid physical parameters needs to be considered. To this end, this paper introduces a heat transfer model in the wellbore.

Two heat transfer mechanisms determine the variation in the annulus temperature: the radial annulus-formation heat exchange and the axial heat convection within the fluid, as shown in Fig. 2. According to the energy conservation equation, the heat transfer mechanism model of the annulus fluid is (Sun et al., 2018):

$$\sum_i A\rho_i\alpha_i C_{pi}\frac{\partial T}{\partial t} + v_m\frac{\partial T}{\partial z} = \frac{T_e - T}{A_0} + \frac{T_p - T}{B_0},\quad i = g,\ L \tag{13}$$

As shown in Fig. 2, considering the variation in the annulus area and the surrounding temperature, the cement ring and casing are treated as a whole, and A_0 can be expressed as a piecewise function (Hasan et al., 2002):

$$A_0 = \begin{cases} \dfrac{1}{2\pi r_{ri}U_a}, & H \le H_w \\[2ex] \dfrac{1}{2\pi}\left(\dfrac{\lambda_f + r_{ci}U_a T_D}{r_{ci}U_a\lambda_f}\right), & H > H_w \end{cases} \tag{14}$$

with

$$U_a^{-1} = \begin{cases} \dfrac{r_{ro}}{r_{ri}h_c} + \dfrac{r_{ro}}{\lambda_r\ln(r_{ro}/r_{ri})} + \dfrac{1}{h_{sea}}, & H \le H_w \\[2ex] \dfrac{r_{co}}{r_{ci}h_c} + \dfrac{r_{co}}{\lambda_c\ln(r_{co}/r_{ci})} + \dfrac{1}{\lambda_{ce}\ln(r_{wb}/r_{co})}, & H > H_w \end{cases} \tag{15}$$

Similarly, the heat transfer resistance B_0 between the annulus and the drill string can be expressed as (Hasan et al., 2002):

$$B_0 = \frac{1}{2\pi r_{pi}U_p} \tag{16}$$

with

$$U_p^{-1} = \frac{r_{po}}{r_{pi}h_{pi}} + \frac{r_{po}}{\lambda_p\ln(r_{po}/r_{pi})} + \frac{1}{h_{po}} \tag{17}$$

where T_D is the dimensionless temperature equation of the formation, which can be calculated using the Hasan's model (Hasan and Kabir, 1991).

Since the drill string is generally equipped with a single-flow valve, the gas cannot enter the drill string during gas kick. Therefore, the fluid inside the drill string is pure liquid phase, and the heat transfer mechanism model is:

$$A\rho_L\alpha_L C_{pL}\frac{\partial T_p}{\partial t} + v_L\frac{\partial T_p}{\partial z} = -\frac{T_p - T}{B_0} \tag{18}$$

The above Eqs. (13) and (18) constitute the thermodynamic model of the wellbore fluid, and can be used to calculate the wellbore temperature distribution.

The above hydrodynamic and thermodynamic models can be discretized using an explicit difference scheme for solution, in which the first-order upwind scheme is used in space and the forward Euler method is used in time. The specific discretization forms can be referred to the relevant literature (Ambrus et al., 2016).
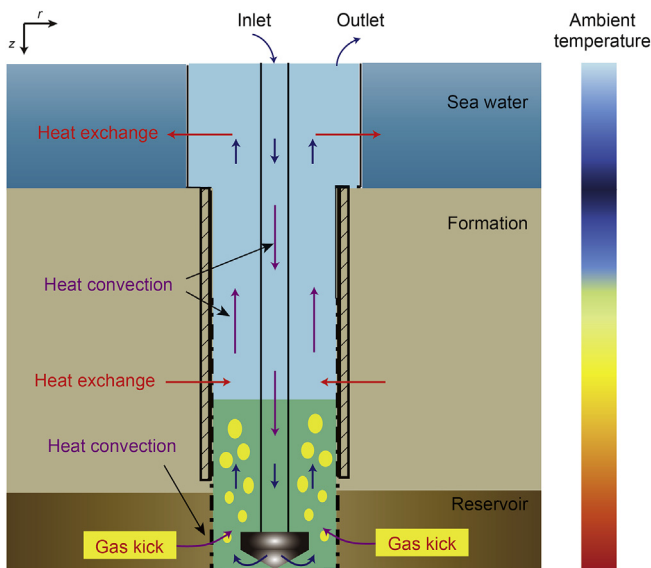
3.3. Auxiliary equation

3.3.1. Gas kick rate

When drilling to an abnormal high-pressure gas reservoir, if the formation pore-pressure exceeds the bottomhole pressure, the gas will break through the mud cake and enter the bottomhole, resulting in a gas kick. Here, a transient porous flow model of the formation gas is employed to evaluate the gas kick rate (Sun et al., 2017), i.e.

$$q_g(h,t) = \frac{2\pi K h \left[P_e^2 - P_b^2(t) \right]}{\mu \ln \frac{2.25 K t / \mu_g C_t}{r_w^2}} \frac{T z_g}{P_b z_e T_e} \rho_g \tag{19}$$

3.3.2. Choke pressure drop

The choke is the key to the dynamic MPWC method. The fluid passing through the choke during well control may be single liquid phase flow or multiphase flow. The flow rate is an equation of the choke coefficient, choke opening, and fluid physical parameters. Based on the mass conservation law, the choke pressure drop model under gas–liquid two-phase flow condition can be expressed as (Ambrus et al., 2016):

$$m_c = \frac{C_v z_{op}}{\sqrt{\rho_L}} \sqrt{P_c - P_s} + \left[\left(1 - \sqrt{\frac{\rho_g}{\rho_L}} \frac{1}{Y} \right) A v_g \alpha_g \right] \tag{20}$$

3.3.3. Interphase slip relation coefficient

In drift flow model, the gas distribution coefficient c_0 and gas slip rate v_∞ are related to the gas fraction and flow rate. According to the studies of Caetano et al. (1992) and Hasan and Kabir (1988), gas–liquid two-phase flow patterns could be classified into five categories: bubble flow, dispersed bubble flow, slug flow, churn Flow and annular flow. The gas distribution coefficient c_0 and gas slip rate v_∞ used in the wellbore multiphase simulator are categorized into two types: integrated model and unified model. The unified model can be used independent of the flow patterns, while the integrated model is not. The integrated model depending on the flow pattern has been used successfully by Hasan et al. (2010) for modeling two phase flows. The transition boundaries and the parameter values of drift-flux model for each specific flow pattern are not completely consistent. Shi et al. (2005) developed a unified model of the distribution coefficients c_0 and the slip rate v_∞ for gas–liquid two-phase flow, based on a large number of experimental results. The calculated results of this model are continuous and accurate, which have been fully confirmed in a large number of previous gas–liquid two-phase flow studies. Shi's model is adopted here. The gas distribution coefficient c_0 is:

$$c_0 = \frac{A_e}{1 + (A_e - 1)\chi^2} \tag{21}$$

The gas slip rate v_∞ is:

$$v_\infty = \frac{c_0 v_c (1 - \alpha_g c_0) K(\alpha_g)}{1 - \alpha_g c_0 \left[1 - (\rho_g / \rho_L)^{1/2} \right]} (\cos\theta)^{1/2} (1 + \sin\theta)^2 \tag{22}$$

4. Model verification

The above model was verified using the measured data from Lage's full-scale experiment (Lage et al., 2003). The experimental well has a vertical depth of 1275 m. The inner diameter of the casing was 159.4 mm, and the outer diameter of the drill string was 88.9 mm. A pressure sensor was installed at a depth of 605 m to measure the annulus pressure. The liquid medium was the water with a displacement of 10.11 m³/s. The gas medium was the nitrogen, which was injected into the annulus through a parasitic pipeline with an inner diameter of 51.8 mm. The depth of the gas injection point was 760 m.

The variation in the gas injection rate in the experiment is shown in Fig. 3. Before injecting gas into the wellbore, the gas was pressurized in the parasitic pipeline until its pressure reached a value that allowed the gas to enter the annulus. As the gas continued to enter the annulus, the annulus pressure decreased gradually, resulting in a gradual increase in gas injection rate. However, when gas front was transported out of the wellhead, the gas flow rate started to decrease gradually until a pseudo-steady state of the gas–liquid two-phase flow was reached in the wellbore.

Fig. 4 presents a comparison between the calculated pressures and the measurement pressure. In the early stage of gas injection ($t < 400$ s), the calculated pressures of this model and the Lage's model agreed well with the measured pressure. During $t = 400-650$ s, the calculated pressures of these two models deviated slightly from the measured pressure, both being slightly smaller than the measured pressure. This was mainly because of the prediction error of the gas–liquid two-phase flow pattern due to the gradual increase in the gas fraction in the wellbore. After $t = 650$ s, the consistency between the calculated pressures and the measured pressure became better again.

Therefore, the calculated pressure of this model agreed well with the measured pressure and the calculated result of Lage's model, which verified the accuracy and reliability of the non-isothermal drift flow simplification model in this paper.

5. Results and discussion

After the model was verified, a series of numerical calculations were carried out to reveal the response characteristics of the outlet flow and the wellhead backpressure during MPWC in deepwater drilling.

In the simulation, the pit gain was used to detect the gas kick, and the gas kick could be identified when the pit gain exceeded
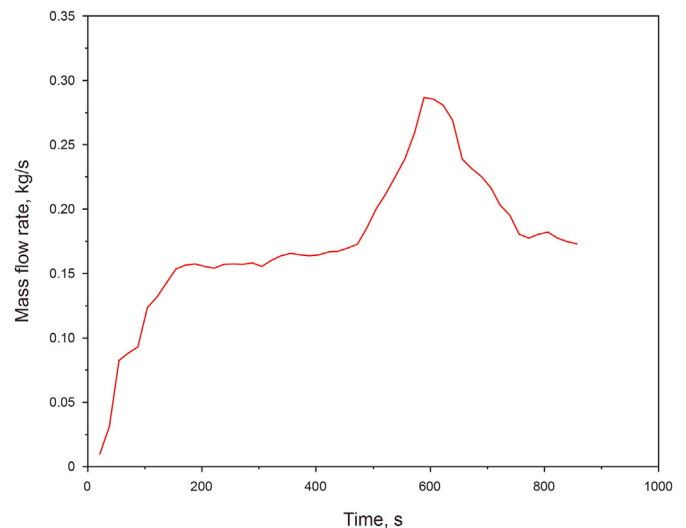

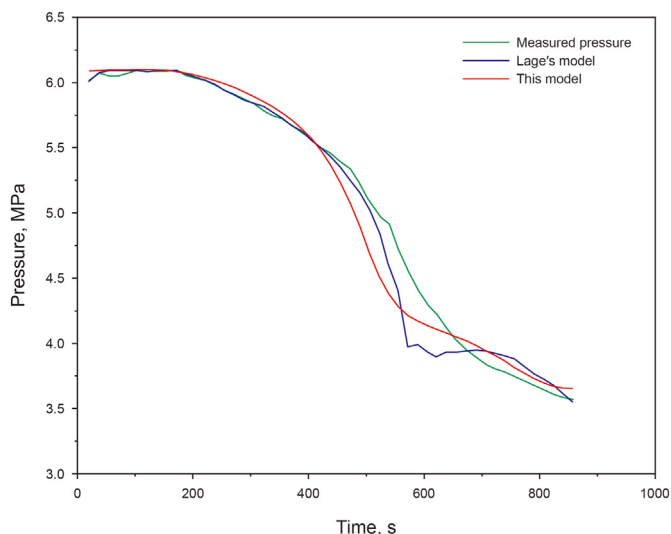**Fig. 3.** Mass flow rate of gas injected in the experiment.

Fig. 4. Comparison of calculated pressures and the experimental pressure.

1 m^3. At this time, the wellhead backpressure began to increase, and the initial increased wellhead backpressure made the bottomhole pressure higher than the formation pore-pressure by 0.5 MPa. The formation pore-pressure was 50 MPa, and the initial wellhead backpressure was 1 MPa during normal drilling without gas kick. Set the initial zero moment as the start time of the gas kick. Other basic parameters were summarized in Table 1.

5.1. Variation in the wellbore multiphase flow state

The state of gas moved in the annulus during dynamic deepwater MPWC is shown in Fig. 5. Before the gas kick was detected, the gas continued to invade into the bottomhole and flow upward along the mud. The invading gas replaced the corresponding volume of mud out of the wellhead, resulting in a gradual decrease in bottomhole pressure. Therefore, the gas kick rate increased gradually, so as the gas fraction in the wellbore, as shown in Fig. 5(a). After the gas kick was identified, the wellhead backpressure was rapidly increased, so that the bottomhole-formation pressure reached a new equilibrium relationship and the gas kick stopped. After this, the gas was gradually circulated out of the wellbore, but the evolution law of the gas in the wellbore was complex and could be divided into four stages.

- Stage I: The gas migrated in the annulus of the formation section before entering the riser, as shown in Fig. 5(a). When the gas—liquid mixture was near the bottomhole, the gas expansion effect was not obvious under the condition of high wellbore pressure, and the slip rate of the gas front was larger than that of the gas back edge. Therefore, the length of gas—liquid mixture

gradually increased, while the gas fraction at each well depth gradually decreased. Then, as the gas moved upwards, the wellbore pressure decreased and the gas expansion effect intensified, resulting in a gradual increase in both the length of gas—liquid mixture and the gas fraction at each well depth.
- Stage II: The gas—liquid mixture passed through the annulus with a large-variable-diameter and gradually entered the riser, as shown in Fig. 5(a) and (b). In this stage, a maximum value of the gas fraction occurred between before and after most of the gas entered the riser. Before most of the gas entered the riser, the migration rate of the gas front was obviously reduced due to the sudden increase in the riser diameter, and was smaller than that of the gas back edge. As a result, the length of the gas—liquid mixture gradually decreased, while the gas fraction at each well depth gradually increased. After most of the gas entered the riser, the large diameter riser and the low temperature near the seabed resulted in a gradual decrease in both the length of gas—liquid mixture and the gas fraction.
- Stage III: The gas moved in the riser before the gas front reached the wellhead, as shown in Fig. 5(b). As the gas moved upwards, the wellbore temperature gradually increased while the wellbore pressure gradually decreased, causing the gas expansion effect to intensify. Therefore, both the length of gas—liquid mixture and the gas fraction gradually increased.
- Stage IV: The gas was gradually discharged out of the wellbore, as shown in Fig. 5(b). Before most of the gas was discharged out of the wellhead, the gas expanded violently and the gas fraction increased sharply due to the low pressure at the wellhead. When most of the gas was discharged, the gas content in the wellbore gradually decreased until the gas was completely discharged.

5.2. Response characteristics of the pit gain and outlet flow rate

Fig. 6 illustrates the variation in the pit gain and outlet flow rate during dynamic deepwater MPWC. Formation gas continuously invaded into the bottomhole before the gas kick was detected, causing the pit gain and outlet liquid flow rate to gradually increase. Here, the pit gain of 1 m^3 was used as the threshold value for gas kick detection. When gas kick was identified, the wellhead backpressure was increased rapidly and the gas was compressed, resulting in a brief reduction in pit gain and outlet liquid flow rate. The variation in outlet liquid flow rate during subsequent gas discharging was closely related to the state of gas transportation in the annulus, and also determined the variation in the pit gain.

When the gas migrated in the annulus of the formation section before entering the riser ($t < 0.80$ h), the gas expansion increased the gas volume in the wellbore, resulting in a gradual increase in the outlet liquid flow rate. Before most of the gas entered the riser (0.80 h $\leq t < 1.14$ h), the gas expansion in the annulus of the formation played a dominant role. However, the dominant role was

Table 1
Basic parameters used in the calculation.

| Parameter	Value	Parameter	Value
Well depth, m	4500	Seawater depth, m	1500
Drilling fluid density, kg/m^3	1200	Drilling fluid viscosity, Pa s	0.054
Surface temperature, °C	20	Inlet temperature, °C	25
Geothermal gradient, °C/m	0.024	Pump rate, m^3/s	0.03
Reservoir permeability, μm^2	0.03	Rate of penetration, m/h	6
Inner diameter of the drill string, mm	127	Outer diameter of the drill string, mm	149.2
Inner diameter of the riser, mm	508	Inner diameter of the casing, mm	244.5
Drill bit diameter, mm	215.9		
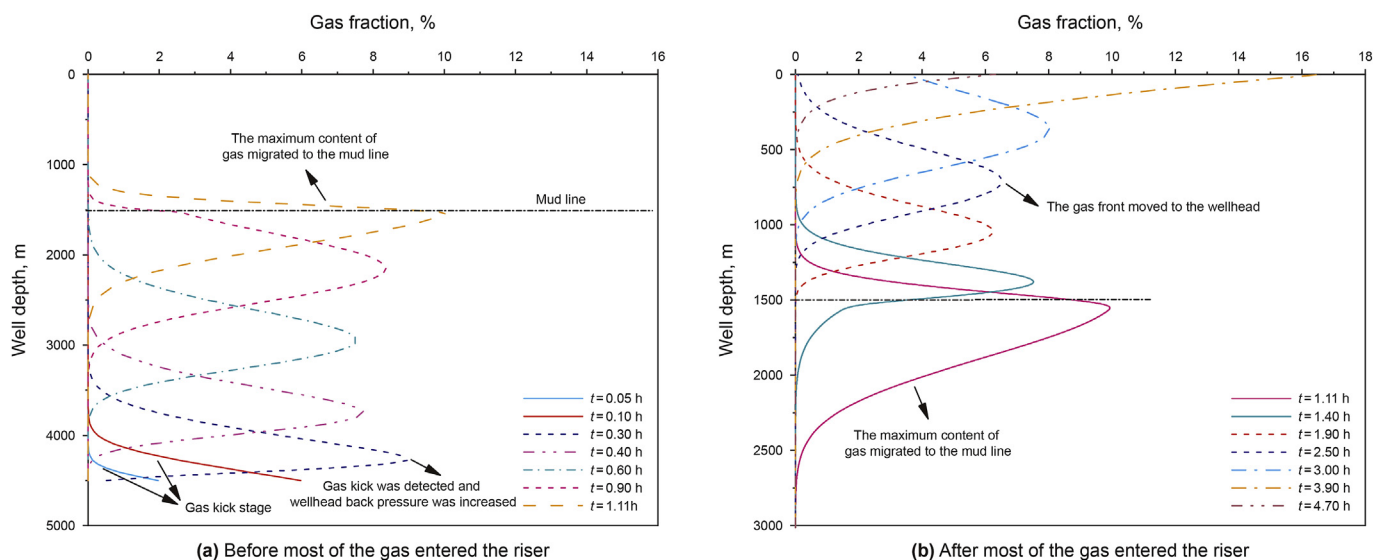
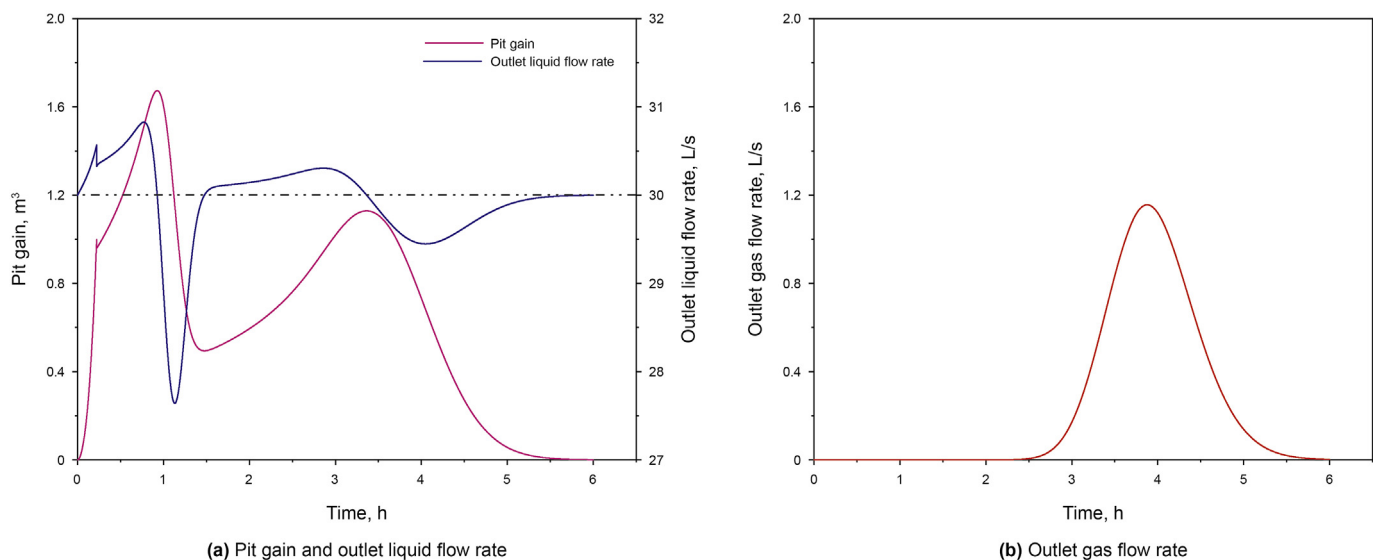**Fig. 5.** The state of gas moved in the annulus during dynamic deepwater MPWC.

Fig. 6. Variation in the outlet flow rate and pit gain.

gradually weakened, while the influence of the gas fraction reduction caused by the large-diameter riser gradually increased. As a result, the outlet liquid flow rate decreased rapidly during this period and eventually it was lower than the inlet flow rate. During most of the gas entering the riser (0.14 h $\leq t <$ 2.89 h), the gas expansion in the riser gradually became the main factor, so that the outlet liquid flow rate gradually increased and eventually exceeded the inlet flow rate. When the gas was gradually discharge out of the wellhead (2.89 h $\leq t <$ 5.62 h), The gas volume first expanded rapidly and then decreased gradually, causing the outlet liquid flow rate to gradually decrease and then return to the same as the inlet flow rate and outlet gas flow rate to gradually increase first and then gradually reduce to zero. The maximum outlet gas flow rate was 1.2 L/s and it was not a large enough flow rate to cause the failure of the surface manifold, mainly due to the fact that MPWC was able to start the gas discharging when the gas influx was small. Also, it could be seen from the outlet gas flow rate that the time for the gas to reach the wellhead was $t =$ 2.49 h.

The variation in the outlet liquid flow rate determined the variation in the pit gain. When the outlet liquid flow rate was greater than the inlet flow rate, the pit gain increased. On the contrary, the pit gain decreased. Thus, at $t =$ 0.96 h and $t =$ 3.38 h, when the outlet liquid flow rate was equal to the inlet flow rate, the pit gain reached two maximum values. Similarly, the pit gain reached two minimum values at $t =$ 1.49 h and $t =$ 5.62 h. Additionally, as the riser diameter was obviously larger than the borehole diameter, the second maximum value of the pit gain was smaller than the first one.

To sum up, due to the large-variable-diameter annulus, the outlet liquid flow rate would be lower than the inlet flow rate and the pit gain would decrease before the gas front migrated to the wellhead. These phenomena were impossible in the dynamic land MPWC. The complex variation in the outlet liquid flow rate and the pit gain brought a lot of interference to the judgment of downhole working conditions in practical engineering.

5.3. Response characteristics of the wellhead backpressure and the choke opening

The response characteristics of the wellhead backpressure and the choke opening during dynamic MPWC are shown in Fig. 7. Prior to the detection of gas kick, the outlet liquid flow rate gradually increased, so the wellhead backpressure also increased with constant choke opening. After the gas kick was detected, it is necessary to dynamically regulate the wellhead backpressure to establish a new equilibrium between the bottomhole pressure and the formation pressure.

During gas circulating and discharging, when the pit gain increased continuously, it meant that the gas volume in the wellbore continued to increase, while the hydrostatic pressure continued to drop. Therefore, the wellhead backpressure needed to be increased to compensate for the hydrostatic pressure drop. Alternatively, as the pit gain decreased, the wellhead backpressure would decrease accordingly. Therefore, the variation trend of the wellhead backpressure was consistent with that of the pit gain. Once the gas was completely discharged from the wellhead, there was pure drilling fluid in the wellbore, and the backpressure did not change. At this time, the wellhead backpressure was less than the initial increased backpressure. The difference between them was the hydrostatic pressure drop caused by the gas invading into the wellbore when gas kick was detected. Therefore, the large-variable-diameter annulus in deepwater drilling resulted in a complicated gas flow in the wellbore, which in turn resulted in complicated variations in wellhead backpressure and choke opening.

Furthermore, as could be seen from Fig. 7, the variation in choke opening was directly related to the choke pressure, but was also influenced by the gas–liquid two-phase flow. Before a trace amount of gas flowed out of the wellhead ($t < 2.8$ h), the fluid passing through the choke was mainly liquid, so the variation in choke opening was negatively related to the choke pressure. When the gas–liquid two-phase flow passed through the choke, the variations in choke opening and choke pressure drop were affected by the gas. For example, when 2.8 h $< t <$ 3.4 h, although the choke opening was increasing, the choke pressure was still increasing. Similarly, when 4.0 h $< t <$ 5.6 h, although the choke opening was decreasing, the choke pressure was also gradually decreasing. This was mainly because the gas would expand or compress in the choke, which caused a portion of the choke pressure drop to be added or unloaded, slowing down the response rate of the wellhead backpressure.
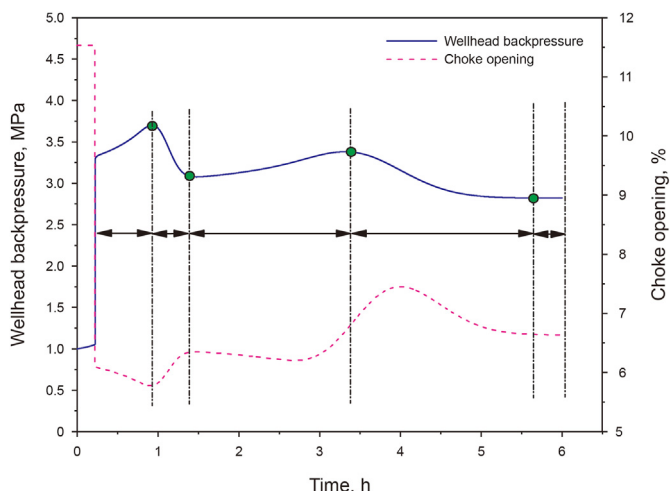
5.4. Response characteristics of the bottomhole pressure and the gas kick rate

The variation in bottomhole pressure and gas kick rate during dynamic MPWC is shown in Fig. 8. Before the gas kick was detected, the gas kick rate gradually increased as the thickness of the uncovered reservoir increased and the bottomhole pressure gradually decreased. After the detection of the gas kick, the dynamic control of wellbore pressure included two stages: (i) Adjust the choke opening to increase the wellhead backpressure, so that the bottomhole pressure was slightly higher than the formation pressure. Here, the bottomhole pressure was set to be 0.5 MPa higher than the formation pressure; (ii) Control the wellhead backpressure to keep the bottomhole pressure constant and circulate the gas out of the wellbore. Therefore, the key of dynamic MPWC was how to control the wellhead backpressure so that the bottomhole pressure was always within the safe density window, which was usually judged by whether the inlet and outlet liquid flow rates were equal (Bacon et al., 2012).

5.5. Sensitivity analysis

In order to fully grasp the influence of large-variable-diameter annulus and complex temperature environment on the response characteristics of outlet flow and wellhead backpressure during dynamic deepwater MPWC, a sensitivity analysis of the relevant parameters was performed below.

5.5.1. Effect of wellbore temperature

Fig. 9 illustrates the effect of wellbore temperature on the response characteristics of outlet flow and wellhead backpressure during dynamic MPWC. The comparison object of this model was that the entire wellbore temperature was the seawater surface temperature, which meant that the actual wellbore temperature of the formation section was obviously higher than the comparison object, and the actual temperature of the riser annulus was lower than the comparison object. The comparison results revealed that the effect of wellbore temperature was manifested in two ways.

On the one hand, the wellbore temperature could affect the expansion effect of the gas. The high formation temperature made the gas expansion effect in the formation annulus more distinct. As a result, the pit gain reached 1 m^3 earlier, shortened the time for gas kick detection. Additionally, before a large amount of gas entered the riser, the gas expansion led to a larger peak of the pit gain and
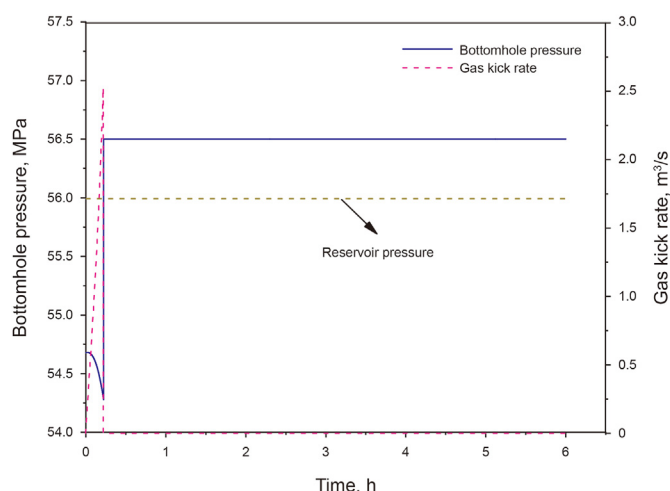

Fig. 7. Response characteristics of the wellhead backpressure and the choke opening.

Fig. 8. Variation in bottomhole pressure and gas kick rate with time.

(a) Outlet liquid flow rate

(b) Outlet gas flow rate

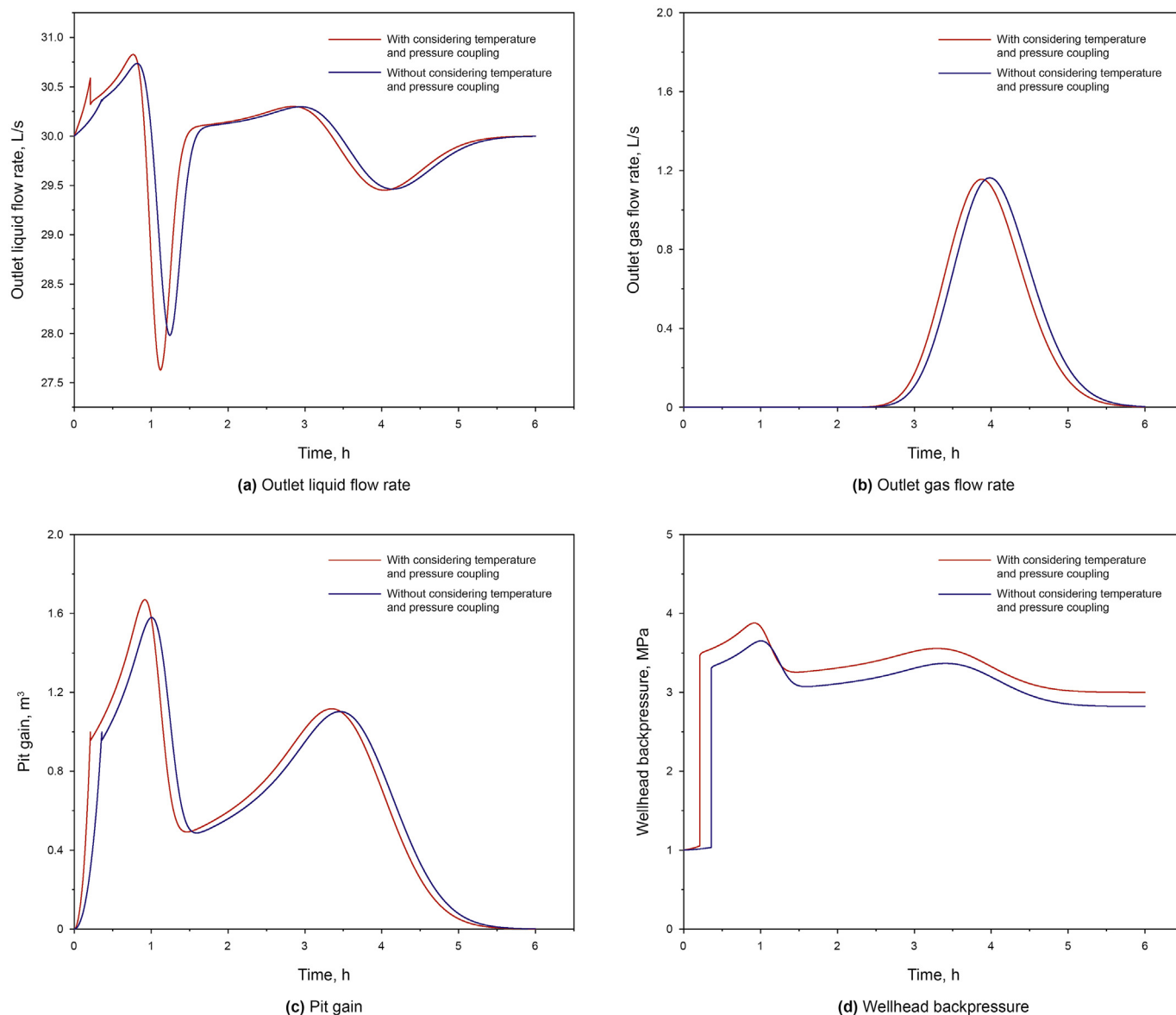(c) Pit gain

(d) Wellhead backpressure

Fig. 9. Effect of the wellbore temperature on the response characteristics of outlet flow and wellhead backpressure.

outlet liquid flow rate. However, when most of the gas gradually entered the riser, the low seawater temperature reduced the gas fraction, resulting in a faster reduction in the outlet liquid flow rate and the pit gain. During the subsequent gas discharging, the two opposite scenarios that occurred earlier offset each other. Therefore, the pit gain and outlet liquid/gas flow rate were approximately the same with and without considering the wellbore temperature, but the gas reached the wellhead faster when temperature was considered, as shown in Fig. 9(a)–(c).

On the other hand, the high temperature environment of the formation wellbore made the drilling fluid density smaller than that without considering the wellbore temperature, so the wellhead backpressure of the former was larger during dynamic MPWC, as shown in Fig. 9(d).

5.5.2. Effect of large-variable-diameter annulus

The effect of large-variable-diameter annulus on the response characteristics of outlet flow and wellhead backpressure was shown in Fig. 10. The model was compared to a case where the

annulus diameter was constant throughout the wellbore, which was also the case in previous studies (Davoudi et al., 2011; Jiang et al., 2019; Kinik et al., 2014; Liao et al., 2020; Smith and Patel, 2012). The variation in outlet liquid/gas flow rate, pit gain and wellhead backpressure calculated by this model was more complex compared to the comparison object. Before the gas front reached the wellhead, there was a phenomenon that the outlet liquid flow rate was less than the inlet flow rate and the pit gain was reduced. In addition, when considering the large-variable-diameter annulus, the gas circulation time was longer, but the fluctuation range in outlet liquid/gas flow rate, pit gain and wellhead backpressure was obviously smaller. From Fig. 10(b), it could be seen more clearly that when the gas front with considering the large-variable-diameter annulus was not yet transported to the wellhead, the gas without considering this condition had been completely discharged from the wellbore. Moreover, the later outlet gas flow rate was nearly three times larger than the former. The initial increased wellhead backpressure and the final wellhead backpressure calculated by this model were both larger, mainly due to the relatively small
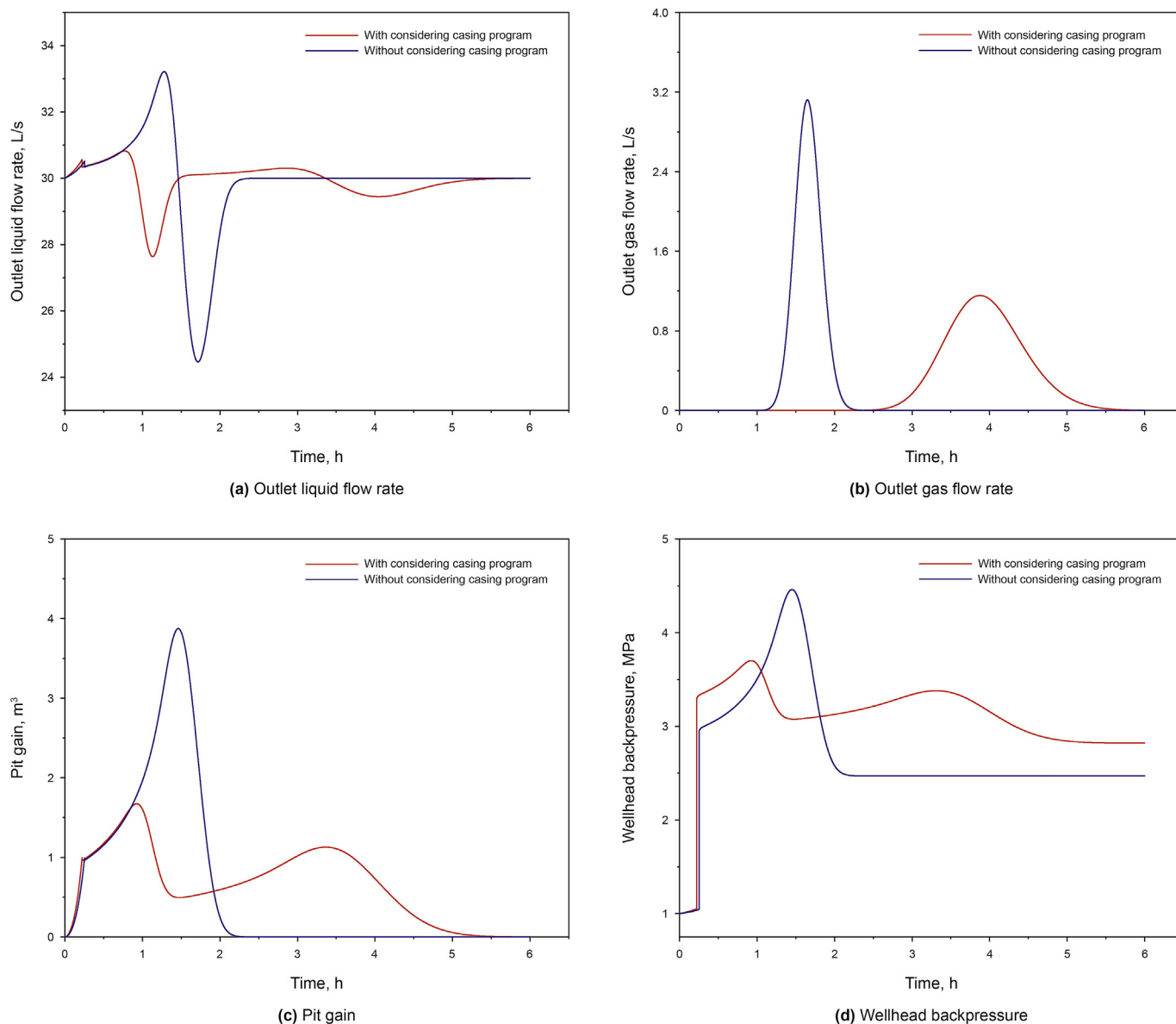
Fig. 10. Effect of the large-variable-diameter annulus on the response characteristics of outlet flow and wellhead backpressure.

annulus pressure loss in the large-diameter riser.

5.5.3. Effect of borehole diameter in the formation section

Fig. 11 shows the effect of borehole diameter in the formation section on the response characteristics of outlet flow and wellhead backpressure. Due to the early gas kick detection, the borehole diameter in the formation section had little effect on the pit gain and outlet liquid flow rate during gas kick. When gas kick was detected, the annulus pressure loss gradually decreased as the borehole diameter in the formation section increased, so the initially increased wellhead backpressure gradually increased, as shown in Fig. 11(d). Additionally, Before the gas front moved to the wellhead, the fluctuation range of outlet liquid flow rate gradually decreased with the increase in borehole diameter in the formation section, while the fluctuation range of pit gain and wellhead backpressure gradually decreased in the early stage and then increased in the later stage. This was because the larger the borehole diameter in the formation section, the smaller the annulus

flow rate and the sudden change in annulus diameter, and the stronger the expansion effect of the gas. During the gas discharging from the wellhead, the more the accumulated gas volume in the wellbore in the early stage, the larger the variation range of outlet liquid/gas flow rate, pit gain, and wellhead backpressure.

5.5.4. Effect of seawater depth

Fig. 12 presents the effect of seawater depth on the response characteristics of outlet flow and wellhead backpressure. The seawater depth determined the riser length, which actually reflected the effect of the position of the sudden change in annulus diameter. The smaller the seawater depth, the longer the distance the fluid flowed in the formation annulus and the larger the annulus pressure loss, so the smaller the initial increased wellhead backpressure and the final wellhead backpressure, as shown in Fig. 12(d). In addition, before the gas front was transported to the wellhead, the smaller the seawater depth, the larger the gas expansion. Therefore, as the seawater depth decreased, the
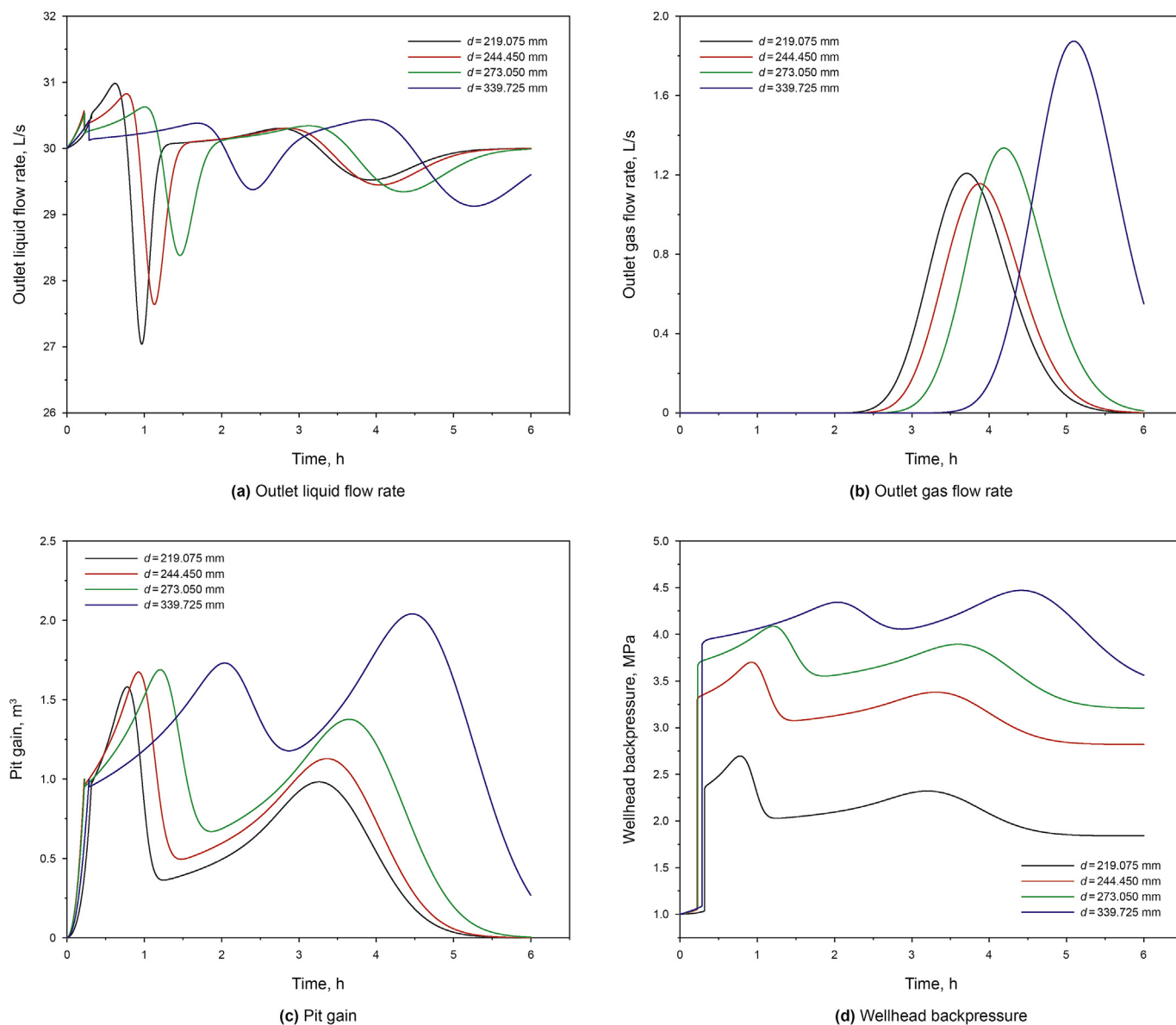
Fig. 11. Effect of borehole diameter in the formation section on the response characteristics of outlet flow and wellhead backpressure.

fluctuation range of the outlet liquid flow rate increased, along with the maximum pit gain and the maximum wellhead backpressure. Similarly, during the gas discharging from the wellhead, the larger the accumulated gas volume in the early stage, the larger the variation range of the outlet liquid/gas flow rate, pit gain and wellhead backpressure in this stage.

5.6. Discussion

In the above, we investigated the dynamic MPWC method for rapid treatment of gas influx in deepwater MPD, mainly considering the effect of the large-variable-diameter annulus and the special temperature distribution environment of deepwater drilling and simplifying the conventional drift flow model considering the computational efficiency. This research could provide a good theoretical guidance for the treatment of gas influx in deepwater MPD. However, there are still some limitations of our model that need to be further investigated, mainly including the following: (1) The heat sources of wellbore fluids include, in addition to

geothermal energy, heat generated by drill bits, torque, frictions loss from hydraulics, and heat carried by formation gas entering the wellbore. How to accurately characterize these heat sources in gas–liquid two-phase flow and take them into account in the thermodynamic model is necessary. (2) The oil or synthetic-based drilling fluid is used in most cases in deepwater drilling. When formation gas enters the wellbore, all or part of the gas will be dissolved, which in turn has a significant effect on the wellbore gas–liquid two-phase flow state. Most existing models that have considered gas dissolution are based on flash model or empirical gas solubility equations, which are difficult to characterize the unsteady gas–liquid interphase mass transfer. (3) There are a lot of CO_2 gas influx, as we are doing the carbon sequestration. CO_2 gas will dissolve in water-based drilling fluid, which is similar to methane gas dissolved in oil-based drilling fluid. However, for oil-based drilling fluid, high concentration of CO_2 gas can lead to changes in fluid properties, such as thickening of oil-based drilling fluid, thereby affecting wellbore multiphase flow characteristics. This is a more complex issue, and no specific research results have
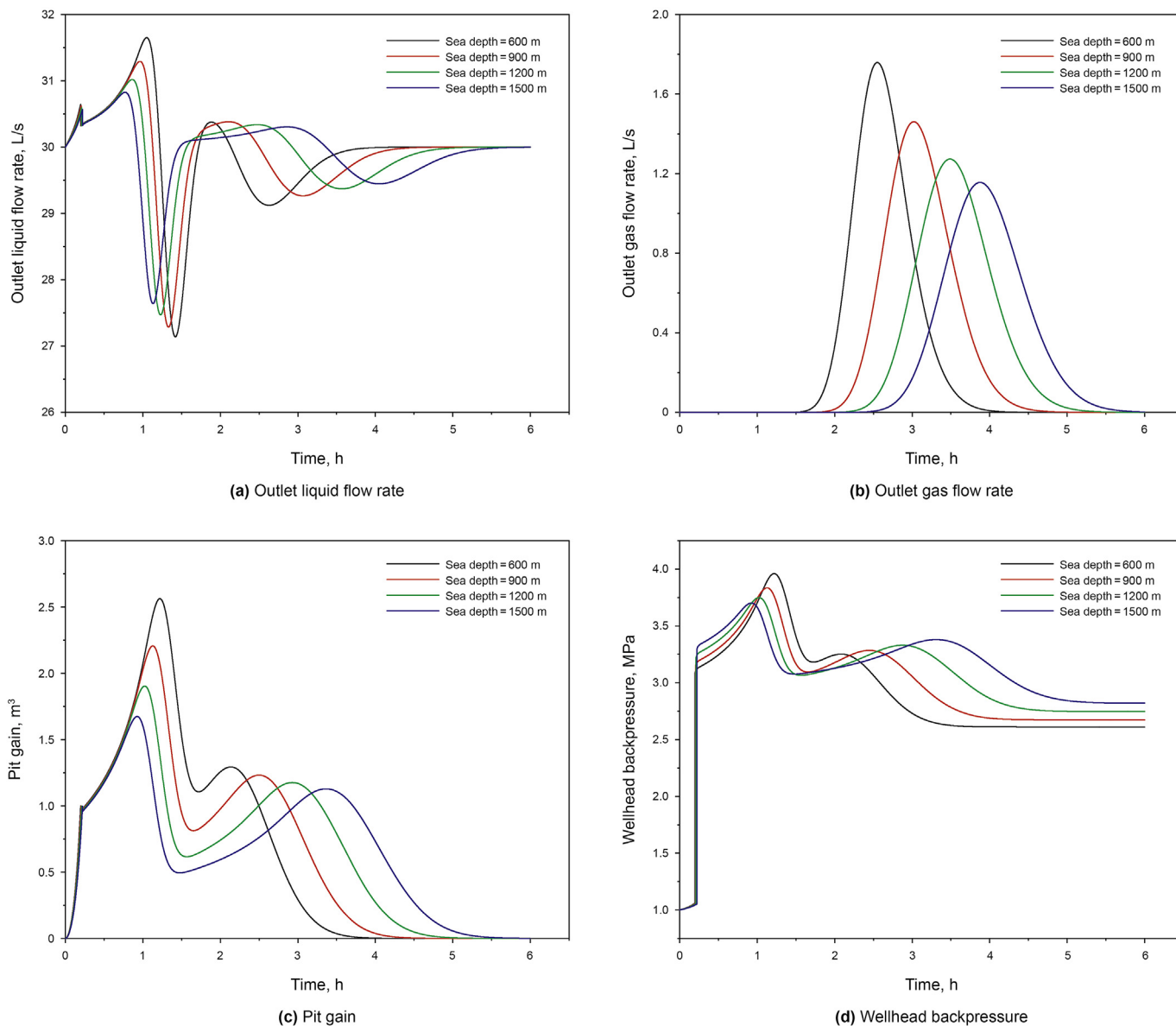
Fig. 12. Effect of seawater depth on the response characteristics of outlet flow and wellhead backpressure.

been seen so far.

6. Conclusions

Combining the characteristics of large-variable-diameter annulus and complex temperature distribution in deepwater drilling, a non-isothermal drift flow simplification model was developed to investigate the response characteristics of outlet flow and wellhead backpressure during dynamic MPWC. The main conclusions include:

(1) Due to the large-variable-diameter annulus in deepwater drilling, the gas fraction and the length of the gas–liquid mixture present complex alternating characteristics when the gas migrates upwards in the wellbore during dynamic MPWC.

(2) The complex gas–liquid two-phase flow in the wellbore indictates that the pit gain and outlet liquid flow rate are also complex and variable. The outlet liquid flow rate will be lower than the inlet flow rate and the pit gain will decrease before the gas moves to the wellhead.

(3) The variation trend of the wellhead backpressure is consistent with that of the pit gain. And the variation in choke opening is obviously affected by the gas–liquid two-phase flow. The expansion and compression of the gas result in a portion of the choke pressure drop being added or unloaded, slowing down the response rate of the wellhead backpressure.

(4) The high formation temperature results in a large gas expansion in deepwater drilling, while the effect of the low seawater temperature offsets that of the high formation temperature. Therefore, the pit gain and outlet liquid flow rate are sensitive to the wellbore temperature in the early stage of gas discharging, while the sensitivity is no longer obvious in the later stage. Meanwhile, the high formation temperature reduces the drilling fluid density, leading to a larger wellhead backpressure during dynamic MPWC.

(5) The borehole diameter in the formation section and the seawater depth respectively determine the amount and position of the sudden change in annulus diameter, and thus have a large effect on the outlet liquid flow rate, pit gain and wellhead backpressure.

Declaration of interest statement

Appendix A. Derivation of the simplified gas−liquid two-phase flow model

The derivation starts from the classical two-phase drift-flow equation that takes into account the flow channel area. The classical transient drift flow model includes the continuity equation and the momentum conservation equation for each phase, in which the independent momentum conservation equations of the gas and liquid are replaced by the mixed gas−liquid momentum conservation equation. The fully transient drift flow model can be formulated as:

$$\frac{\partial}{\partial t}(A\rho_g\alpha_g) + \frac{\partial}{\partial z}(A\rho_g\alpha_g v_g) = m_g \tag{A.1}$$

$$\frac{\partial}{\partial t}(A\rho_L\alpha_L) + \frac{\partial}{\partial z}(A\rho_L\alpha_L v_L) = 0 \tag{A.2}$$

$$\frac{\partial}{\partial t}\left(\sum_i A\rho_i\alpha_i v_i\right) + \frac{\partial}{\partial z}\left(\sum_i A\rho_i\alpha_i v_i^2\right) + \frac{\partial}{\partial z}(AP) = S, \quad i = g, \ L \tag{A.3}$$

with

$$S = -2Af\frac{\rho_m v_m |v_m|}{d_c} - A\rho_m g\sin\theta \tag{A.4}$$

$$\rho_m = \alpha_g\rho_g + \alpha_L\rho_L \tag{A.5}$$

$$v_m = \alpha_g v_g + \alpha_L v_L \tag{A.6}$$

The volume fractions of gas and liquid satisfy:

$$\alpha_g + \alpha_L = 1 \tag{A.7}$$

The gas equation of state can be used to determine the gas density:

$$P = \rho_g z_g R_g T \tag{A.8}$$

The gas−liquid slip relationship is able to completely characterize the mutual interaction mechanism of the gas and liquid. The gas−liquid slip relationship can be described as (Choi et al., 2007):

$$v_g = c_0 v_m + v_\infty \tag{A.9}$$

In order to facilitate the derivation of the simplified drift flow model, the slip relationship between gas and liquid is deformed and Eq. (A.9) can be expressed as (Aarsnes et al., 2016a):

$$v_g = \frac{v_m}{1 - \alpha_L^*} + v_\infty \tag{A.10}$$

where $\alpha_L^* = (c_0 - 1)/c_0$, $\alpha_L^* \in [0, \ 1)$ and $v_\infty \geq 0$ are constant parameters.

Substituting Eq. (A.10) into Eq. (A.9), the slip relationship can be formulated as:

$$\alpha_L v_L = (\alpha_L - \alpha_L^*)v_g - (1 - \alpha_L^*)v_\infty \tag{A.11}$$

Substituting Eq. (A.11) into Eq. (A.2), with the assumption of constant ρ_L and $\rho_L\frac{\partial}{\partial z}[A(1 - \alpha_L^*)v_\infty] \cong 0$, we get:

$$\frac{\partial(A\alpha_L)}{\partial t} + \frac{\partial[A(\alpha_L - \alpha_L^*)v_g]}{\partial z} = 0 \tag{A.12}$$

which, after employing the chain rule for derivatives, combined with Eq. (A.7), yields:

$$\frac{\partial(A\alpha_g)}{\partial t} + v_g\frac{\partial(A\alpha_g)}{\partial z} - \left[\frac{\partial A}{\partial t} + (1 - \alpha_L^*)v_g\frac{\partial A}{\partial z}\right] = A(\alpha_L - \alpha_L^*)\frac{\partial v_g}{\partial z} \tag{A.13}$$

The wellbore annulus area will be resized only at some locations, so we consider here that $\frac{\partial A}{\partial t} + (1 - \alpha_L^*)v_g\frac{\partial A}{\partial z} \cong 0$. Eq. (A.13) can be simplified as:

$$\frac{\partial(A\alpha_g)}{\partial t} + v_g\frac{\partial(A\alpha_g)}{\partial z} = A(\alpha_L - \alpha_L^*)\frac{\partial v_g}{\partial z} \tag{A.14}$$

From Eq. (A.1), we can apply the chain rule to obtain the following relationship:

$$\frac{\partial v_g}{\partial z} = \frac{m_g}{A\alpha_g\rho_g} - \frac{1}{A\alpha_g}\left[\frac{\partial(A\alpha_g)}{\partial t} + v_g\frac{\partial(A\alpha_g)}{\partial z}\right] - \frac{1}{\rho_g}\left(\frac{\partial\rho_g}{\partial t} + v_g\frac{\partial\rho_g}{\partial z}\right) \tag{A.15}$$

Inserting Eq. (A.15) into the right-hand side of Eq. (A.14), after algebraic manipulation, yields:

$$\frac{\partial(A\alpha_g)}{\partial t} + v_g\frac{\partial(A\alpha_g)}{\partial z} = -\frac{A\alpha_g(\alpha_L - \alpha_L^*)}{(1 - \alpha_L^*)\rho_g}\left(\frac{\partial\rho_g}{\partial t} + v_g\frac{\partial\rho_g}{\partial z}\right) + \frac{\alpha_L - \alpha_L^*}{(1 - \alpha_L^*)\rho_g}m_g \tag{A.16}$$

We define the convenience variable E_g and m_g^*:

$$E_g = -\frac{A\alpha_g(\alpha_L - \alpha_L^*)}{(1 - \alpha_L^*)\rho_g}\left(\frac{\partial\rho_g}{\partial t} + v_g\frac{\partial\rho_g}{\partial z}\right) \tag{A.17}$$

$$m_g^* = \frac{\alpha_L - \alpha_L^*}{(1 - \alpha_L^*)\rho_g}m_g \tag{A.18}$$

Thus, we have from (A.16):

$$\frac{\partial(A\alpha_g)}{\partial t} + v_g\frac{\partial(A\alpha_g)}{\partial z} = E_g + m_g^* \tag{A.19}$$

A.1 Pressure profile

The quasi-steady pressure is obtained from Eq. (A.3), discarding the transient and acceleration terms:

$$\frac{\partial P}{\partial z} = \overline{S}(z) = -\overline{\rho}_m\left(g\sin\theta + \frac{2fv_m|v_m|}{d_c}\right) \tag{A.20}$$

with

$$\overline{\rho}_m = \alpha_L\rho_L + \alpha_g\overline{\rho}_g \tag{A.21}$$

where a mean or approximated gas density $\overline{\rho}_g$ needs to be used since pressure is implicitly dependent on gas density (from Eq. (A.8)). For instance, $\overline{\rho}_g$ may be computed from Eq. (A.8) assuming a linear temperature profile, and the pressure profile at the previous time instant. Integrating Eq. (A.20) from bottomhole ($z = 0$) to the surface ($z = H$) gives:

$$P(z) = P_c + \int_H^z \overline{S}(\xi)d\xi \tag{A.22}$$

A.2 Velocity profile

Using the variables defined in Eqs. (A.17) and (A.18), we can simplify Eq. (A.15) as:

$$\frac{\partial v_g}{\partial z} = \frac{E_g + m_g^*}{A(\alpha_L - \alpha_L^*)} \tag{A.23}$$

The boundary condition for Eq. (A.19), defined at the bottomhole ($z = 0$), is:

$$\alpha(z = 0, t) = \frac{q_g}{Av_{g0}} \tag{A.24}$$

with

$$v_{g0} = v_g(z = 0, t) = c_0\left(\frac{m_g}{A\rho_g} + v_L\right) + v_\infty \tag{A.25}$$

Assuming adiabatic gas expansion, with the specific heat ratio γ, we have the relation:

$$\frac{d\rho_g}{\rho_g} = \frac{dP}{\gamma P} \tag{A.26}$$

where $\gamma = 1$ for the constant temperature, and γ is equal to the adiabatic gas constant for an isentropic process.

Eq. (A.26) allows us to recast Eq. (A.17) in terms of the pressure profile:

$$E_g = -\frac{A\alpha_g(1 - c_0\alpha_g)}{\gamma P}\left[\frac{\partial P}{\partial t} + v_g\frac{\partial P}{\partial z}\right] \tag{A.27}$$

We can also write the mass source term m_g^* as a function of pressure, using the relationship $c_g^2 = \frac{\gamma P}{\rho_g}$:

$$m_g^* = \frac{(1 - c_0\alpha_g)c_g^2}{\gamma P}m_g \tag{A.28}$$

We can further simplify the gas velocity expression (Eq. (A.23)). Using Eqs. (A.27) and (A.28) together with Eq. (A.20), yields:

$$\frac{\partial v_g}{\partial z} = c_0\left(-\frac{\alpha_g}{\gamma P}\frac{\partial P}{\partial t} - \frac{\alpha_g v_g}{\gamma P}\overline{S} + \frac{c_g^2}{A\gamma P}m_g\right) \tag{A.29}$$

If we further neglect $\partial P/\partial t$ when computing the velocity gradient, we have the approximation:

$$\frac{\partial v_g}{\partial z} = c_0\left(-\frac{\alpha_g v_g}{\gamma P}\overline{S} + \frac{c_g^2}{A\gamma P}m_g\right) \tag{A.30}$$

Integrating Eq. (A.30) over the length of the well, we get:

$$v_g(z) = e^{-I_v(z)}\left[v_{g0} + c_0\int_0^z\left(\frac{c_g^2(\xi)m_g(\xi)}{A\gamma P(\xi)}e^{I_v(\xi)}\right)d\xi\right] \tag{A.31}$$

with

$$I_v(z) = \int_0^z\left[\frac{c_0\alpha_g(\xi)}{\gamma P(\xi)}\overline{S}(\xi)\right]d\xi \tag{A.32}$$

A.3 Lumped pressure dynamics

We use a lumped expression for the pressure dynamics. Considering the annulus as a single control volume, and applying the mass conservation law:

$$\frac{\partial P_c}{\partial t} = \frac{\beta}{V}\left(q_L + q_g + T_{EG} - q_c\right) \tag{A.33}$$

The term T_{EG} can be found by integrating the gradient of the gas velocity along the well. Including the $\partial P/\partial t$ term in Eq. (A.29), T_{EG} can be written as:

$$T_{EG} = \int_0^H Ac_0\left(-\frac{\alpha_g(\xi)v_g(\xi)}{\gamma P(\xi)}\overline{S}(\xi) + \frac{c_g^2(\xi)}{A(\xi)\gamma P(\xi)}m_g(\xi)\right)d\xi$$
$$-\frac{dP_c}{dt}\int_0^H A(\xi)\frac{c_0\alpha_g(\xi)}{\gamma P(\xi)}d\xi \tag{A.34}$$

We define:

$$T_{XE} = \int_0^H Ac_0\left(-\frac{\alpha_g(\xi)v_g(\xi)}{\gamma P(\xi)}\overline{S}(\xi) + \frac{c_g^2(\xi)}{A(\xi)\gamma P(\xi)}m_g(\xi)\right)d\xi = A(v_g(H) - v_{g0}) \tag{A.35}$$

and substitute Eqs. (A.34) and (A.35) into Eq. (A.33), we have:

$$\frac{\partial P_c}{\partial t} = \frac{\overline{\beta}}{V} \left(q_L + q_g - q_c + T_{XE} \right) \tag{A.36}$$

with

$$\overline{\beta} = \frac{\beta_L}{1 + \frac{\beta_L}{V} \int_0^H \frac{c_0 \alpha_g(\xi)}{\gamma P(\xi)} \, \mathrm{d}\xi} \tag{A.37}$$

References

Aarsnes, U.J.F., Ambrus, A., Di Meglio, F., Vajargah, A.K., Aamo, O.M., van Oort, E., 2016a. A simplified two-phase flow model using a quasi-equilibrium momentum balance. Int. J. Multiphas. Flow 83, 77−85. https://doi.org/10.1016/j.ijmultiphaseflow.2016.03.017.

Aarsnes, U.J.F., Di Meglio, F., Graham, R., Aamo, O.M., 2016b. A methodology for classifying operating regimes in underbalanced-drilling operations. SPE J. 21 (2), 423−433. https://doi.org/10.2118/178920-PA.

Ambrus, A., Aarsnes, U.J.F., Vajargah, A.K., Akbari, B., 2016. Real-time estimation of reservoir influx rate and pore pressure using a simplified transient two-phase flow model. J. Nat. Gas Sci. Eng. 32, 439−452. https://doi.org/10.1016/j.jngse.2016.04.036.

Avelar, C.S., Ribeiro, P.R., Sepehrnoori, K., 2009. Deepwater gas kick simulation. J. Petrol. Sci. Eng. 67 (1−2), 13−22. https://doi.org/10.1016/j.petrol.2009.03.001.

Bacon, W., Tong, A., Gabaldon, O., Sugden, C., Suryanarayana, P., 2012. An improved dynamic well control response to a gas influx in managed pressure drilling operations. In: IADC/SPE Drilling Conference and Exhibition. https://doi.org/10.2118/151392-MS.

Baer, M.R., Nunziato, J.W., 1986. A two-phase mixture theory for the deflagration-to-detonation transition (DDT) in reactive granular materials. Int. J. Multiphas. Flow 12 (6), 861−889. https://doi.org/10.1016/0301-9322(86)90033-9.

Caetano, E.F., Shoham, O., Brill, J.P., 1992. Upward vertical two-phase flow through an annulus—part i: single-phase friction factor, Taylor bubble rise velocity, and flow pattern prediction. J. Energy Resour. Technol. 114 (1), 1−13. https://doi.org/10.1115/1.2905917.

Choe, J., 2001. Advanced two-phase well control analysis (May). J. Can. Petrol. Technol. 40 (5). https://doi.org/10.2118/01-05-02.

Choi, J., Pereyra, E., Sarica, C., Lee, H., Jang, I.S., Kang, J., 2007. Analyses and procedures for kick detection in subsea mudlift drilling. SPE Drill. Complet. 22 (4), 296−303. https://doi.org/10.2118/87114-PA.

Choi, J., Pereyra, E., Sarica, C., Lee, H., Jang, I.S., Kang, J., 2013. Development of a fast transient simulator for gas—liquid two-phase flow in pipes. J. Petrol. Sci. Eng. 102, 27−35. https://doi.org/10.1016/j.petrol.2013.01.006.

Das, A.K., Smith, J.R., Frink, P.J., 2008. Simulations comparing different initial responses to kicks taken during managed pressure drilling. In: IADC/SPE Drilling Conference. https://doi.org/10.2118/112761-MS.

Davoudi, M., Smith, J.R., Patel, B.M., Chirinos, J.E., 2011. Evaluation of alternative initial responses to kicks taken during managed-pressure drilling. SPE Drill. Complet. 26 (2), 169−181. https://doi.org/10.2118/128424-PA.

Flatten, T., Lund, H., 2011. Relaxation two-phase flow models and the sub-characteristic condition. Math. Model Methods Appl. Sci. 21 (12), 2379−2407. https://doi.org/10.1142/S0218202511005775.

Flores, J.G., Sarica, C., Chen, T.X., Brill, J.P., 1998. Investigation of holdup and pressure drop behavior for oil-water flow in vertical and deviated wells. J. Energy Resour. Technol. 120 (1), 8−14. https://doi.org/10.1115/1.2795016.

Guner, H., 2009. Simulation Study of Emerging Well Control Methods for Influxes Caused by Bottomhole Pressure Fluctuations during Managed Pressure Drilling. M.S. Thesis. Louisiana State University, US.

Hasan, A., Kabir, C.S., 1991. Heat transfer during two-phase flow in wellbores; Part I–formation temperature. In: SPE Annual Technical Conference and Exhibition. https://doi.org/10.2118/22866-MS.

Hasan, A.R., Kabir, C.S., 1988. A study of multiphase flow behavior in vertical wells. SPE Prod. Eng. 3 (2), 263−272. https://doi.org/10.2118/15138-PA.

Hasan, A.R., Kabir, C.S., Sarica, C., 2002. Fluid Flow and Heat Transfer in Wellbores. Society of Petroleum Engineers, Richardson, Texas.

Hasan, A.R., Kabir, C.S., Sayarpour, M., 2010. Simplified two-phase flow modeling in wellbores. J. Petrol. Sci. Eng. 72 (1−2), 42−49. https://doi.org/10.1016/j.petrol.2010.02.007.

He, M., Liu, G., Li, J., Li, J., Zhang, T., Liu, W., Li, M., 2015. Study of sour gas kicks taken during managed pressure drilling operations. In: SPE/IATMI Asia Pacific Oil & Gas Conference and Exhibition. https://doi.org/10.2118/176337-MS.

Jiang, H., Liu, G., Li, J., Zhang, T., Wang, C., Ren, K., 2019. Numerical simulation of a

new early gas kick detection method using UKF estimation and GLRT. J. Petrol. Sci. Eng. 173, 415−425. https://doi.org/10.1016/j.petrol.2018.09.065.

Kaasa, G.-O., Stamnes, O.N., Lmsland, L., Aamo, O.M., 2012. Simplified hydraulics model used for intelligent estimation of downhole pressure for a managed-pressure-drilling control system. SPE Drill. Complet. 27 (1), 127−138. https://doi.org/10.2118/143097-PA.

Kinik, K., Gumus, F., Osayande, N., 2014. A case study: first field application of fully automated kick detection and control by MPD system in western Canada. In: SPE/IADC Managed Pressure Drilling & Underbalanced Operations Conference & Exhibition. https://doi.org/10.2118/168948-MS.

Lage, A., Fjelde, K.K., Time, R.W., 2003. Underbalanced drilling dynamics: two-phase flow modeling and experiments. SPE J. 8 (1), 61−70. https://doi.org/10.2118/143097-PA.

Leblanc, J., Lewis, 1968. A mathematical model of a gas kick. J. Petrol. Technol. 20 (8), 888−898. https://doi.org/10.2118/1860-PA.

Liao, Y., Sun, X., Sun, B., Wang, Z., Zhang, J., Lou, W., 2020. Wellhead backpressure control strategies and outflow response characteristics for gas kick during managed pressure drilling. J. Nat. Gas Sci. Eng. 75, 103164. https://doi.org/10.1016/j.jngse.2020.103164.

Ma, Z., Vajargah, A.K., Chen, D., Van Oort, E., May, R., MacPherson, J.D., 2018. Gas kicks in non-aqueous drilling fluids: a well control challenge. In: IADC/SPE Drilling Conference and Exhibition. https://doi.org/10.2118/189606-MS.

Manikonda, K., Hasan, A.R., Kaldirim, O., Schubert, J.J., Rahman, M.A., 2019. Understanding gas kick behavior in water and oil-based drilling fluids. In: SPE Kuwait Oil & Gas Show and Conference. https://doi.org/10.2118/198069-MS.

Manikonda, K., Hasan, A.R., Barooah, A., Rahmani, N.H., El-Naas, M., Sleiti, A.K., Rahman, M.A., 2020. A mechanistic gas kick model to simulate gas in a riser with water and synthetic-based drilling fluid. In: Abu Dhabi International Petroleum Exhibition & Conference. https://doi.org/10.2118/203159-MS.

Manikonda, K., Hasan, A.R., Rahmani, N.H., Kaldirim, O., Obi, C.E., Schubert, J.J., Rahman, M.A., 2021. A gas kick model that uses the thermodynamic approach to account for gas solubility in synthetic-based mud. In: SPE/IADC Middle East Drilling Technology Conference and Exhibition. https://doi.org/10.2118/202152-MS.

Nayeem, A.A., Venkatesan, R., Khan, F., 2016. Monitoring of down-hole parameters for early kick detection. J. Loss. Prevent. Proc. 40, 43−54. https://doi.org/10.1016/j.jlp.2015.11.025.

Nickens, 1987. A dynamic computer model of a kicking well. SPE Drill. Eng. 2 (2), 159−173. https://doi.org/10.2118/14183-PA.

Nunes, J., Bannwart, A., Ribeiro, P., 2002. Mathematical modeling of gas kicks in deep water scenario. In: IADC/SPE Asia Pacific Drilling Technology. https://doi.org/10.2118/77253-MS.

Petalas, N., Aziz, K., 2000. A mechanistic model for multiphase flow in pipes. J. Can. Petrol. Technol. 39 (6), 43−55. https://doi.org/10.2118/00-06-04.

Ramos, J.I., 1995. One-dimensional, time-dependent, homogeneous, two-phase flow in volcanic conduits. Int. J. Numer. Methods Fluid. 21 (3), 253−278. https://doi.org/10.1002/fld.1650210306.

Randolph, M.F., Gaudin, C., Gourvenec, S.M., White, D.J., Boylan, N., Cassidy, M.J., 2011. Recent advances in offshore geotechnics for deep water oil and gas developments. Ocean. Eng. 38 (7), 818−834. https://doi.org/10.1016/j.oceaneng.2010.10.021.

Rommetveit, R., Vefring, E., 1991. Comparison of results from an advanced gas kick simulator with surface and downhole data from full scale gas kick experiments in an inclined well. In: SPE Annual Technical Conference and Exhibition. https://doi.org/10.2118/22558-MS.

Santos, O.L.A., 1991. Well-control operations in horizontal wells. SPE Drill. Eng. 6 (2), 111−117. https://doi.org/10.2118/21105-PA.

Shi, H., Holmes, J.A., Durlofsky, L.J., Aziz, K., Diaz, L., Alkaya, B., 2005. Drift-flux modeling of two-phase flow in wellbores. SPE J. 10 (1), 24−33. https://doi.org/10.2118/84228-PA.

Smith, J.R., Patel, B.M., 2012. A proposed method for planning the best initial response to kicks taken during managed-pressure-drilling operations. SPE Drill. Complet. 27 (2), 194−203. https://doi.org/10.2118/143101-PA.

Sule, I., Imtiaz, S., Khan, F., Butt, S., 2019. Nonlinear model predictive control of gas kick in a managed pressure drilling system. J. Petrol. Sci. Eng. 174, 1223−1235. https://doi.org/10.1016/j.petrol.2018.11.046.

Sule, I., Khan, F., Butt, S., Yang, M., 2018. Kick control reliability analysis of managed pressure drilling operation. J. Loss. Prevent. Proc. 52, 7−20. https://doi.org/10.1016/j.jlp.2018.01.007.

Sun, B., Sun, X., Wang, Z., Chen, Y., 2017. Effects of phase transition on gas kick migration in deepwater horizontal drilling. J. Nat. Gas Sci. Eng. 46, 710−729. https://doi.org/10.1016/j.jngse.2017.09.001.

Sun, X., Sun, B., Gao, Y., Wang, Z., 2018. A model of multiphase flow dynamics considering the hydrated bubble behaviors and its application to deepwater kick simulation. J. Energ. Resour-Asme. 140 (8). https://doi.org/10.1115/1.4040190.

Vajargah, A.K., van Oort, E., 2015. Early kick detection and well control decision-making for managed pressure drilling automation. J. Nat. Gas Sci. Eng. 27, 354−366. https://doi.org/10.1016/j.jngse.2015.08.067.

Wang, C., Liu, G., Yang, Z., Li, J., Zhang, T., Jiang, H., 2020. Downhole gas-kick transient simulation and detection with downhole dual-measurement points in water-based drilling fluid. J. Nat. Gas Sci. Eng. 84, 103678. https://doi.org/10.1016/j.jngse.2020.103678.

Yang, H., Li, J., Liu, G., Jiang, H., Wang, C., Jiang, J., 2019a. A transient hydro-thermo-bubble model for gas kick simulation in deep water drilling based on oil-based mud. Appl. Therm. Eng. 158, 113776. https://doi.org/10.1016/j.applthermaleng.2019.113776.

Yang, H., Li, J., Liu, G., Wang, C., Jiang, H., Luo, K., Wang, B., 2019b. A new method for early gas kick detection based on the consistencies and differences of bottomhole pressures at two measured points. J. Petrol. Sci. Eng. 176, 1095−1105. https://doi.org/10.1016/j.petrol.2019.02.026.

Yang, H., Li, J., Liu, G., Xing, X., Jiang, H., Wang, C., 2020. The effect of interfacial mass transfer of slip-rising gas bubbles on two-phase flow in the vertical wellbore/pipeline. Int. J. Heat Mass Tran. 150, 119326. https://doi.org/10.1016/j.ijheatmasstransfer.2020.119326.

Yin, B., Liu, G., Li, X., 2017. Multiphase transient flow model in wellbore annuli during gas kick in deepwater drilling based on oil-based mud. Appl. Math. Model. 51, 159−198. https://doi.org/10.1016/j.apm.2017.06.029.